

CHEMISTRY

A European Journal

A Journal of



Accepted Article

Title: Preassembled Coumarin-Rhodamine Scaffold for Ratiometric Sensing of Nitric Oxide and Hypochlorite

Authors: Jun Xiang Ong, Victoria Yu Ting Pang, Li Min Tng, and Wee Han Ang

This manuscript has been accepted after peer review and appears as an Accepted Article online prior to editing, proofing, and formal publication of the final Version of Record (VoR). This work is currently citable by using the Digital Object Identifier (DOI) given below. The VoR will be published online in Early View as soon as possible and may be different to this Accepted Article as a result of editing. Readers should obtain the VoR from the journal website shown below when it is published to ensure accuracy of information. The authors are responsible for the content of this Accepted Article.

To be cited as: *Chem. Eur. J.* 10.1002/chem.201703554

Link to VoR: <http://dx.doi.org/10.1002/chem.201703554>

Supported by
ACES

WILEY-VCH

Preassembled Coumarin-Rhodamine Scaffold for Ratiometric Sensing of Nitric Oxide and Hypochlorite

Jun Xiang Ong,^[a] Victoria Yu Ting Pang,^[a] Li Min Tng,^[a] and Wee Han Ang^{*[a, b]}

[a] *J. X. Ong, V. Y. T. Pang, L. M. Tng, Prof. W. H. Ang*

Department of Chemistry, National University of Singapore, 3 Science Drive 3, Singapore 117543 (Singapore)

E-mail: chmawh@nus.edu.sg

[b] *Prof. W. H. Ang*

NUS Graduate School for Integrative Sciences and Engineering, National University of Singapore, 28 Medical Drive, Singapore 117456 (Singapore)

Abstract: A new preassembled ratiometric sensing platform was constructed from a coumarin donor and a rhodamine acceptor designed for through-bond energy transfer (TBET). A phenylacetylene linker was installed to disrupt the planarity of the extended conjugated system but retaining the efficient energy transfer between the donor and acceptor motifs. To demonstrate its versatility as a sensing platform, we conjugated recognition motifs through amide coupling reactions to yield two TBET chemosensors capable of sensing either endogenously produced NO and ClO⁻. Both probes possessed high selectivity for their analytes, exhibited good stability under physiological conditions, and performed well as bioimaging probes in living cells.

Introduction

In the past few decades, fluorescent probes based on small organic molecules have emerged as powerful tools to study biomolecules and biologically-relevant metal ions in living systems. These small-molecule fluorescent dyads have been widely employed in bioimaging owing to their high sensitivity, selectivity and high spatial and temporal resolution.^[1] However, most of these probes function via changes to the intensity of a single emission signal. Hence, intensity-based probes tend to be affected by factors such as variations in probe concentrations, excitation intensities and environmental effects. To overcome challenges associated with intensity-based probes, researchers have developed probes which can emit at two different emission wavelengths. By taking the intensity ratios of the different emissions, these ratiometric probes provide a built-in correction for the above-mentioned effects.^[2] Förster Resonance Energy Transfer (FRET) is a mechanism commonly adopted for the design of ratiometric fluorescent probes. In a FRET system, the donor and acceptor fluorophores are linked via non-conjugated spacers and energy transfer from the donor to acceptor occurs through space. A substantial spectral overlap between the emission spectrum of the donor and the absorption spectrum of the acceptor is required for efficient energy transfer to take place but it limits the choice of donor and acceptor fluorophores available.^[3] There has been a growing interest in fluorescent probes based on Through Bond Energy Transfer (TBET). As opposed to FRET, donor and acceptor fluorophores are linked via electronically conjugated spacers in TBET systems and energy transfer occurs through the conjugated bond without the need for spectral overlap.^[4] This unique feature endows TBET fluorescent probes with high energy transfer efficiencies and large pseudo-Stokes shifts.

TBET ratiometric chemosensors utilizing bright fluorogenic rhodamine acceptor scaffolds have been reported for the detection of various analytes and their designs can be broadly divided into two main strategies. In one strategy, the donor and acceptor motifs are not electronically-conjugated when the rhodamine acceptor is in its inactivated closed-ring form. Upon activation e.g. detection of an analyte, spiro-ring opening occurs on the rhodamine scaffold enabling TBET via electronic conjugation.^[5] In these designs, donor molecules are typically incorporated as part of the sensing mechanism for the analytes which makes the probe susceptible to decomposition. A more desirable strategy would be to construct TBET chemosensors from pre-assembled TBET ratiometric scaffolds and to install the sensing mechanism at the last synthesis step. Few such TBET ratiometric scaffolds have been reported. For example, Xiao and co-workers successfully

fabricated two ratiometric fluorescent probes for the detection of mercury ions and nitric oxide based on a phenyl-linked BODIPY-rhodamine TBET scaffold.^[6] Peng and co-workers developed a naphthalimide-rhodamine TBET platform and applied it for sensing of copper ions.^[7] Tan and co-workers developed two-photon naphthalene-rhodamine TBET chemosensors for imaging of copper and palladium ions in living cells and tissues.^[8] Apart from the aforementioned TBET platforms, a handful of pre-assembled platforms based on FRET have also been developed for the detection of an array of analytes.^[9] There is a need to expand the repertoire of ratiometric TBET scaffolds.

Hypochlorous acid (HClO)/hypochlorite (ClO^-) is an important reactive oxygen species (ROS) in living organisms produced by the reaction of hydrogen peroxide and chloride ions catalyzed by myeloperoxidase (MPO).^[10] It plays a key role in host immune defense system and is capable of killing a wide range of pathogens.^[11] Excessive HClO/ ClO^- generation can induce cellular damage leading to cancer, neurodegeneration and cardiovascular diseases.^[12] Nitric oxide (NO), an important signal transduction molecule in pathological and physiological processes, plays a critical role in cell signaling pathways in the central nervous system,^[13] and acts as the endothelium-derived relaxing factor in the cardiovascular system.^[14] Misregulation of NO production is implicated in various pathologies like stroke, heart disease, hypertension and neurodegenerative diseases.^[15] To the best of our knowledge, only one ratiometric probe fabricated from a pre-assembled TBET platform has been reported for NO^[6b] but none reported for ClO^- .

Herein, we report the fabrication of a new coumarin-rhodamine platform designed for TBET as shown in Fig. 1. The donor and acceptor motifs were connected by a phenylacetylene linker to prevent the fragments from adopting planarity and behaving as a single conjugated fluorophore. This was confirmed through computational modeling which showed that the coumarin and rhodamine motifs adopt a twisted conformation favorable for TBET (Fig. S1). To demonstrate the versatility of this new platform, we conjugated *o*-phenylenediamine and benzoylhydrazine as sensing motifs for NO and ClO^- , respectively, to access new ratiometric probes for detection of NO and ClO^- in living cells.

Results and Discussion

Synthesis and Characterization

The coumarin-rhodamine ratiometric fluorescent dyads were prepared in accordance with Scheme 1. The coumarin donor motif was synthesized in 2 steps from 4-bromophenyl-coumarin. 4-bromophenyl-coumarin was treated with trimethylsilylacetylene under Sonogashira coupling conditions with Pd(PPh₃)₂Cl₂ and CuI as co-catalysts to afford 4-(trimethylsilyl)-phenylacetylene-coumarin in moderate yield. Deprotection of 4-(trimethylsilyl)-phenylacetylene-coumarin with TBAF gave 4-phenylacetylene-coumarin in good yield. Conjugation of 4-phenylacetylene-coumarin to 5'-Br-Rhodamine B via Sonogashira coupling afforded the TBET ratiometric platform **1** in moderate yield. **1** was treated sequentially with POCl₃ and *o*-phenylenediamine or benzoylhydrazine to prepare target compounds **1·NO** and **1·ClO**, respectively, and were fully characterized by NMR and ESI-MS.

Photophysical properties and sensing responses of probes

We investigated for the photophysical properties and sensing responses. Firstly, the absorption and emission properties of **1·NO** was examined in CH₃CN/PBS buffer (v/v=4:6, 2 mM, pH 7.4) as shown in Fig. 2 (Fig. S2). Untreated **1·NO** displayed an absorption band centered at 420 nm which can be attributed to the characteristic absorption peak of the coumarin donor. Since the rhodamine acceptor was in the closed-ring form, no absorption band of rhodamine was observed. Upon addition of DEA NONOate (a commercially-available NO precursor), a new absorption band centered at 555 nm appeared gradually indicating an NO-induced spiro ring opening reaction leading to the formation of the rhodamine chromophore. In addition, an obvious colour change from yellow to pink was observed (Fig. 3). Similar to the absorption studies, upon excitation at 420 nm, untreated **1·NO** displayed only a single emission band centered at 505 nm which can be ascribed to the emission of coumarin donor. In the presence of increasing amounts of NO (0–50 eq.), the intensity of the emission band at 505 nm decreased in intensity and simultaneously a new emission band at 580 nm that gradually increased in intensity was observed. This observation can be attributed to the energy transfer from coumarin (donor) to rhodamine (acceptor) following ring opening of the spiro lactam induced by NO. Consistently, the emission colour of the solution turned from bluish-green to orange-red (Fig. 3). The ratio of emission intensities of rhodamine to coumarin (I_{580}/I_{505}) increased steadily with addition of increasing amounts of NO and good

linearity was established between the emission ratios and NO concentrations from 0–500 μM , suggesting that it is potentially useful for the quantitative determination of NO. The detection limit $(3\sigma/\text{slope})^{[16]}$ for NO was determined to be 0.73 μM . The energy transfer efficiency was determined to be 81.5%, which was comparable to literature reports (Fig. S3).^[7] Time-dependent fluorescence response studies carried out revealed that the fluorescence intensity ratios increased gradually in a linear fashion over time in the presence of NO and plateaued after 100 min (Fig. S4).

The photophysical characteristics of **1·ClO** was expected to be similar to **1·NO** (Fig. 2, S5). With increasing amounts of NaClO (0–10 eq.), **1·ClO** displayed similar trends upon probe activation with good linearity within the biologically-relevant range of 0–200 μM . The limit of detection $(3\sigma/\text{slope})$ of **1·ClO** was determined to be 0.41 μM . Notably, time-dependent fluorescence response showed that the emission ratio reached a plateau within 2 min after the addition of NaClO (Fig. S6). This indicated that **1·ClO** could respond rapidly towards NaClO making the probe an ideal tool for real-time imaging. Thus, we demonstrated that with our single pre-assembled TBET ratiometric platform, we could generate at least two new chemosensors for the ratiometric detection of NO and ClO⁻.

Selectivity and pH response of probes

Since biological systems contain a complex mixture of different reactive oxygen species (ROS), reactive nitrogen species (RNS) and metal ions, it is imperative that chemosensors have the abilities to detect target analytes without interference of other species commonly present in such biological systems. We examined the selectivity of the probes in presence of various ROS and RNS such as NO₂⁻, NO₃⁻, H₂O₂, ·OH, *t*BuOOH and O₂⁻, as well as metal ions such as Na⁺, K⁺, Mg²⁺, Cu²⁺, Ni²⁺, Zn²⁺, Fe²⁺ and Fe³⁺. As shown in Fig. 4 (Fig. S7, S8), the presence of other biological relevant species did not induce any changes to the fluorescence intensity ratios of **1·NO** and **1·ClO**, revealing excellent selectivity towards NO and ClO⁻, respectively. The high selectivity for NO and ClO⁻ illustrated the potential of the probes for biological applications.

The effect of pH on the fluorescence responses of the probes was also studied. The fluorescence intensity ratios (I_{580}/I_{505}) of untreated **1·NO** and **1·ClO** were not affected by variations in pH values over a large pH range 3–11 as shown in Fig. 4. This showed that the probes existed predominantly in the spirocyclic form in the pH range 3–11 making both probes compatible with physiological

conditions. The activation of the probes in the presence of NO and ClO⁻ is pH dependent, with notable enhancement of fluorescence responses observed in the range of pH 3–9 for **1•NO** and pH range of 5–11 for **1•ClO** compared to the free probes in buffer solutions. Since intracellular pH typically ranges from 5–8, **1•NO** and **1•ClO** are expected to work in a cellular environment with negligible background fluorescence.

Detection mechanisms of NO and ClO⁻

We postulated that the chemosensors were activated via spiroring-opening followed by cleavage of the recognition motif to yield scaffold **1**, triggering a fluorogenic response. The mode of action is in keeping with previous reports. NO oxidises **1•NO** to form an acylbenzotriazole intermediate which decomposed in aqueous solution to yield **1** (Fig. S9).^[17] Similarly, **1•ClO** first formed a diacyl diimide intermediate upon oxidation by ClO⁻ followed by aqueous decomposition to **1** (Fig. S10).^[18] During the activation process, the probes were converted from the closed-ring to the opened-ring form, allowing energy transfer to occur. To validate the proposed mechanisms, we employed mass spectrometry to study plausible reaction products. Solutions of **1•NO** and **1•ClO** after treatment with DEA NONOate and NaClO, respectively, were analyzed using ESI-MS. In both instances, a single peak of *m/z* 758.4 was observed which corresponded to the formation of **1** (*m/z* 758.4 [M+H]⁺) (Fig. S11, S12). This is in good agreement with the absorption and emission studies pointing to the formation of a common reaction product **1** upon treatment of the respective probes with NO and ClO⁻.

Detection of exogenous NO and ClO⁻ in cells via fluorescence imaging

To demonstrate the potential application of **1•NO** and **1•ClO** in biological systems, both probes were applied for ratiometric fluorescence imaging in living cells. HeLa cells were incubated with either **1•NO** (10 μM) or **1•ClO** (20 μM) in culture medium for 30 min at 37 °C. The cells treated with the probes showed strong intracellular fluorescence arising from coumarin at λ₅₀₅ and negligible emission from rhodamine at λ₅₈₀ indicating the cell membrane was permeable to the probes and that they were stable under intracellular conditions. Upon treatment with DEA NONOate (100 μM) for 2 h and NaClO (100 μM) for 1 h, a significant increase in λ₅₈₀ was observed accompanied by a decrease in λ₅₀₅ (Fig. 5, S13). This phenomenon was in good

agreement with the emission profiles of **1•NO** and **1•ClO** in aqueous solutions in the presence of NO and ClO⁻, respectively.

Detection of endogenous NO and ClO⁻ in RAW 264.7 cells via fluorescence imaging

The promising results of exogenous NO and ClO⁻ ratiometric imaging in living cells prompted us to investigate the feasibility of these probes in the detection of endogenous analytes. Murine RAW 264.7 macrophages were chosen as the imaging model as they can be stimulated by the treatment of lipopolysaccharides (LPS) and 12-myristate-13-acetate (PMA) to produce endogenous ClO⁻ in immune systems. In contrast, LPS and interferon- γ (IFN- γ) can stimulate macrophages to produce NO. RAW 264.7 macrophage cells treated with probes only displayed intense emission at λ_{505} and negligible emission at λ_{580} . After treatment with LPS (1 $\mu\text{g mL}^{-1}$) for 12 h and then further co-incubation with PMA (1 $\mu\text{g mL}^{-1}$) and **1•ClO** (20 μM) for 12 h at 37 °C, decreased λ_{505} emission and a marked enhancement at λ_{580} was observed (Fig. 6). Similarly, co-incubation of macrophage cells with LPS (1 $\mu\text{g mL}^{-1}$), IFN- γ (1000 U mL^{-1}) and **1•NO** (10 μM) for 12 h at 37 °C exhibited a similar profile (Fig. S14). Taken together, these data showed that the probes are capable of detecting endogenously produced NO and ClO⁻ in living cells.

Conclusion

In summary, we have successfully developed two ratiometric probes specific to NO and ClO⁻ based on a new TBET scaffold constructed from coumarin and rhodamine fluorophores. Both probes demonstrated high selectivity over a panel of biologically-relevant ROS, RNS and metal ions. The probes are stable over a wide pH range and possess good ratiometric fluorescence turn-on ratios for detection of NO and ClO⁻ at physiological pH. They are cell permeable and can be applied for the ratiometric fluorescence imaging of exogenous and endogenous NO and ClO⁻ in living cells. The modular nature of this new TBET scaffold opens the door to a wider variety of ratiometric fluorescent sensors by simply conjugating other recognition motifs of interest.

Experimental Section

Materials and instrumentation

All reagents were purchased from commercial vendors and used without further purification. 5'-Br-Rhodamine B was synthesized according to literature methods.^[19] ¹H NMR spectra were recorded on a Bruker Advance 300 MHz model. Chemical shifts are reported in parts per million relative to residual solvent peaks. Electro-spray ionization mass spectrometry spectra were obtained on a Thermo Finnigan MAT ESI-MS system. UV-vis spectra were recorded on a Shimadzu UV-1800 UV-vis spectrophotometer. Emission fluorescence spectra were recorded on a JOBIN YVON Fluorolog by HORIBA with iHR320 detector. Fluorescence images were captured with Olympus FluoView FV1000 (Olympus, Japan) laser scanning confocal microscope, with 405 nm laser as the excitation source. Computational modelling was performed using Maestro docking program.

Synthesis of 4-bromophenyl-coumarin

To 4-bromophenylacetic acid (1.20 g, 5.61 mmol) and 4-diethylamino-salicylaldehyde (1.07 g, 5.58 mmol) was added pyridine (451 μ L, 5.58 mmol). The reaction mixture was then dissolved in acetic anhydride (1.05 mL) and refluxed for 12 h. After the reaction, solvent was removed and the crude residue was purified by column chromatography (1:6 v/v ethyl acetate:hexane) to give the product as yellow solid. Yield: 450 mg (21.7%). ¹H NMR (300 Hz, CDCl₃): δ 7.69 (s, 1 H, Ar-H), 7.57 (dd, 4 H, Ar-H), 7.31 (d, 1 H, Ar-H), 6.60 (dd, 1 H, Ar-H), 6.52 (d, 1 H, Ar-H), 3.44 (q, 4 H, -CH₂), 1.22 (t, 6 H, -CH₃).

Synthesis of 4-(trimethylsilyl)-phenylacetylene-coumarin

To 4-bromophenyl-coumarin (330 mg, 0.89 mmol) was added Pd(PPh₃)₂Cl₂ (63 mg, 0.089 mmol), CuI (17 mg, 0.089 mmol), PPh₃ (48 mg, 0.180 mmol) and trimethylsilylacetylene (378 μ L, 2.67 mmol). NEt₃ (5 mL) and THF (25 mL) were then added and the reaction mixture was refluxed for 12 h under an inert N₂ environment. After the reaction, solvent was removed and the crude residue was purified by column chromatography (1:6 v/v ethyl acetate:hexane) to give the product as yellow solid. Yield: 307 mg (88.7%). ¹H NMR (300 Hz, CDCl₃): δ 7.72 (s, 1 H, Ar-H), 7.66 (d, 2 H, Ar-H), 7.51 (d, 2 H, Ar-H), 7.31 (d, 1 H, Ar-H), 6.63 (dd, 1 H, Ar-H), 6.55 (d, 1 H, Ar-H), 3.45 (q, 4 H, -CH₂), 1.23 (t, 6 H, -CH₃), 0.26 (s, 9 H, -CH₃).

Synthesis of 4-phenylacetylene-coumarin

4-(trimethylsilyl)-phenylacetylene-coumarin (265 mg, 0.681 mmol) was dissolved in THF (20 mL) and 1 M TBAF solution in THF (0.681 μ L, 0.681 mmol) was added. The reaction was stirred at r.t. for 0.5 h. After the reaction, solvent was removed and the crude residue was purified by column chromatography (1:3 v/v ethyl acetate:hexane) to give the product as yellow solid. Yield: 174 mg (80.6%). $^1\text{H NMR}$ (300 Hz, CDCl_3): δ 7.72 (s, 1 H, Ar-H), 7.66 (d, 2 H, Ar-H), 7.51 (d, 2 H, Ar-H), 7.31 (d, 1 H, Ar-H), 6.63 (dd, 1 H, Ar-H), 6.55 (d, 1 H, Ar-H), 3.44 (q, 4 H, $-\text{CH}_2$), 3.12 (s, 1 H, $-\text{C}\equiv\text{C}-\text{H}$), 1.23 (t, 6 H, $-\text{CH}_3$).

Synthesis of 1

5'-Br-Rhodamine B (233 mg, 0.448 mmol), 4-phenylacetylene-coumarin (142 mg, 0.448 mmol), $\text{PdCl}_2(\text{PPh}_3)_2$ (32 mg, 0.045 mmol), PPh_3 (23 mg, 0.264 mmol) and CuI (4.4 mg, 0.023 mmol) in THF/ NEt_3 (4:1) (25 mL) were refluxed for 18 h under N_2 . After the reaction, the solvent was removed and the crude residue purified by column chromatography (100% dichloromethane to 250:3:3 v/v dichloromethane:methanol:triethylamine to 95:5 v/v dichloromethane:methanol) to give the product as purple-red solid. Yield: 172 mg (50.6%). $^1\text{H NMR}$ (300 Hz, CDCl_3): δ 7.69 (m, 5 H, Ar-H), 7.47 (d, 2 H, Ar-H), 7.35 (s, 1 H, Ar-H), 7.30 (d, 1 H, Ar-H), 6.70 (d, 2 H, Ar-H), 6.58 (dd, 1 H, Ar-H), 6.49 (m, 3 H, Ar-H), 6.41 (m, 2 H, Ar-H), 3.40 (m, 12 H, $-\text{CH}_2$), 1.19 (m, 18 H, $-\text{CH}_3$). ESI-MS: m/z 758.5 $[\text{M}+\text{H}]^+$.

Synthesis of 1·NO

1 (50 mg, 0.066 mmol) in 1, 2-dichloroethane (12 mL) was added POCl_3 (0.3 mL) dropwise over 5 min. The reaction mixture was left to reflux overnight. After the reaction, the solvent was evaporated to give the crude acid chloride as violet-red oil. The crude acid chloride was dissolved in DCM (8 mL) and added drop-wise to a solution of *o*-phenylenediamine (14.3 mg, 0.132 mmol) and NEt_3 (0.4 mL) in DCM (12 mL). The reaction mixture was stirred at r.t. overnight. After the reaction, the solvent was removed and the crude residue purified by column chromatography (1:1 v/v ethyl acetate:hexane) to give the product as yellow solid. Yield: 20 mg (34.3%). $^1\text{H NMR}$ (300 Hz, CDCl_3): δ 8.05 (d, 1 H, Ar-H), 7.74 (m, 4 H, Ar-H), 7.50 (m, 2 H, Ar-H), 7.44 (s, 3 H, Ar-H), 7.05 (m, 2 H, Ar-H), 6.92 (m, 2 H, Ar-H), 6.60 (m, 2 H, Ar-H), 6.52 (m, 3 H, Ar-H), 6.39 (m, 1

H, Ar-H), 3.43 (q, 12 H, -CH₂), 1.24 (m, 18 H, -CH₃). ESI-MS: *m/z* 874.4 [M+Na]⁺. Anal. Calcd. for C₅₅H₅₃N₅O₄: C 77.90, H 6.30, N 8.26. Found: C 77.65, H 6.64, N 8.57.

Synthesis of 1·ClO

1 (50 mg, 0.066 mmol) in 1, 2-dichloroethane (12 mL) was added POCl₃ (0.3 mL) dropwise over 5 min. The reaction mixture was left to reflux overnight. After the reaction, the solvent was evaporated to give the crude acid chloride as violet-red oil. The crude acid chloride was dissolved in DCM (8 mL) and added drop-wise to a solution of benzoylhydrazine (18 mg, 0.132 mmol) and NEt₃ (0.4 mL) in DCM (12 mL). The reaction mixture was stirred at r.t. overnight. After the reaction, the solvent was removed and the crude residue purified by column chromatography (1:1 v/v ethyl acetate:hexane) to give the product as yellow solid. Yield: 13 mg (22.7%). ¹H NMR (300 Hz, CDCl₃): δ 8.00 (d, 1 H, Ar-H), 7.69 (m, 5 H, Ar-H), 7.51 (m, 6 H, Ar-H), 7.36 (m, 6 H, Ar-H), 6.57 (m, 2 H, Ar-H), 6.40 (bs, 2 H, Ar-H), 3.41 (m, 12 H, -CH₂), 1.18 (m, 18 H, -CH₃) ppm. ESI-MS: *m/z* 876.3 [M+H]⁺. Anal. Calcd. for C₅₆H₅₃N₅O₅: C 76.78, H 6.10, N 7.99. Found: C 77.11, H 6.45, N 8.38.

Fluorescence studies

1·NO and **1·ClO** were dissolved in DMSO to obtain 1 mM stock solutions. For **1·NO**, fluorescence experiments were carried out by incubating the dyad (10 μM) dissolved in CH₃CN/PBS buffer (v/v=4:6, 2 mM, pH 7.4) with various amounts of DEA NONOate prepared freshly in 0.01 M NaOH. For **1·ClO**, fluorescence experiments were carried out by incubating the dyad (20 μM) dissolved in CH₃CN/Tris-HCl buffer (v/v=6:4, 2 mM, pH 7.4) with various amounts of NaClO. The detection limits were calculated based on fluorescence titration experiments. Fluorescence spectra of the probes were measured ten times to obtain standard deviations (σ) of the blank measurements and the slopes were obtained from the plots of intensity ratios against the concentrations of NO or ClO⁻. NaCl, KCl, MgCl₂, CuSO₄, ZnCl₂, FeSO₄ and FeCl₃ were used as the source of metal ions. NO was generated from DEA NONOate, ClO⁻ was generated from aqueous NaClO (4-4.99 % chlorine), NO₂⁻ was generated from NaNO₂, NO₃⁻ was generated from NaNO₃, H₂O₂ was generated from aqueous H₂O₂ (30% w/w), •OH was generated from the Fenton reaction, *t*BuOOH was generated from *t*BuOOH solution (70% wt. in H₂O) and O₂⁻ was generated from KO₂. For **1·NO**, selectivity tests were carried out by incubating the dyad (10 μM) with

various ROS/RNS/metal ions (500 μM). For **1•ClO**, selectivity tests were carried out by incubating the dyad (20 μM) with various ROS/RNS/metal ions (200 μM). pH response studies of the probes were measured from pH 3–11.6 by substituting buffers of different pH while keeping the final buffer concentrations constant. pH 3–6 were measured using 200 mM $\text{CH}_3\text{COOH}/\text{CH}_3\text{COO}^-$ buffer, pH 7.4 was measured using 10 mM PBS buffer or 50 mM Tris-HCl buffer and pH 8.4–11.6 were measured with 100 mM $\text{H}^+/\text{HPO}_4^-$ buffer.

Ratiometric fluorescence imaging of exogenous NO and ClO•

HeLa cells were cultured in Dulbecco's modified Eagle's medium (DMEM) supplemented with 10% FBS and 1% antibiotics at 37 °C with 5 % CO_2 . Cells were seeded on cover slips in 6-well plates at a density of 20×10^4 cells per mL and incubated overnight. The cells were washed with PBS buffer twice and incubated with probes **1•NO** (10 μM) or **1•ClO** (20 μM) at 37 °C. After 30 min, the cells were washed with PBS buffer thrice and incubated with DEA NONOate (100 μM) or NaClO (100 μM) for 1 h and 2 h respectively at 37 °C. Subsequently, the cells were washed with PBS buffer thrice, fixed with 4% paraformaldehyde for 15 min and then washed thrice with PBS buffer. The control experiments were prepared by incubating the cells with probes only at 37 °C for 30 min, washed with PBS buffer thrice, fixed with 4% paraformaldehyde for 15 min and then washed thrice with PBS buffer. The cover slips were mounted onto glass slides in a mounting medium and fluorescence images were acquired with Olympus FluoView FV1000 (Olympus, Japan) laser scanning confocal microscope, with 405 nm laser as the excitation source.

Ratiometric fluorescence imaging of endogenous NO and ClO•

RAW 264.7 macrophage cells were cultured in DMEM supplemented with 10% FBS and 1% antibiotics at 37 °C with 5 % CO_2 . Cells were seeded on cover slips in 6-well plates at a density of 20×10^4 cells per mL and incubated overnight. The macrophage cells were washed twice with PBS buffer and incubated with LPS (1 $\mu\text{g mL}^{-1}$) at 37 °C. After 12 h, the cells were further co-incubated with PMA (1 $\mu\text{g mL}^{-1}$) and **1•ClO** (20 μM) for 12 h at 37 °C. For detection of endogenous NO, the macrophage cells were co-incubated with LPS (1 $\mu\text{g mL}^{-1}$), IFN- γ (1000 U mL^{-1}) and **1•NO** (10 μM) for 12 h at 37 °C. The cells were washed with PBS buffer thrice, fixed with 4% paraformaldehyde for 15 min and then washed thrice with PBS buffer. The control experiment was prepared by incubating the cells with probes only at 37 °C for 12 h, washed with PBS buffer thrice,

fixed with 4% paraformaldehyde for 15 min and then washed thrice with PBS buffer. The cover slips were mounted onto glass slides in a mounting medium and fluorescence images were acquired with Olympus FluoView FV1000 (Olympus, Japan) laser scanning confocal microscope, with 405 nm laser as the excitation source.

Acknowledgements

The authors gratefully acknowledge financial support from Ministry of Education and National University of Singapore (R143-000-680-114). The authors also thank Chemical, Molecular and Materials Analysis Center (CMMAC) for performing elemental analysis experiments.

Conflict of interest

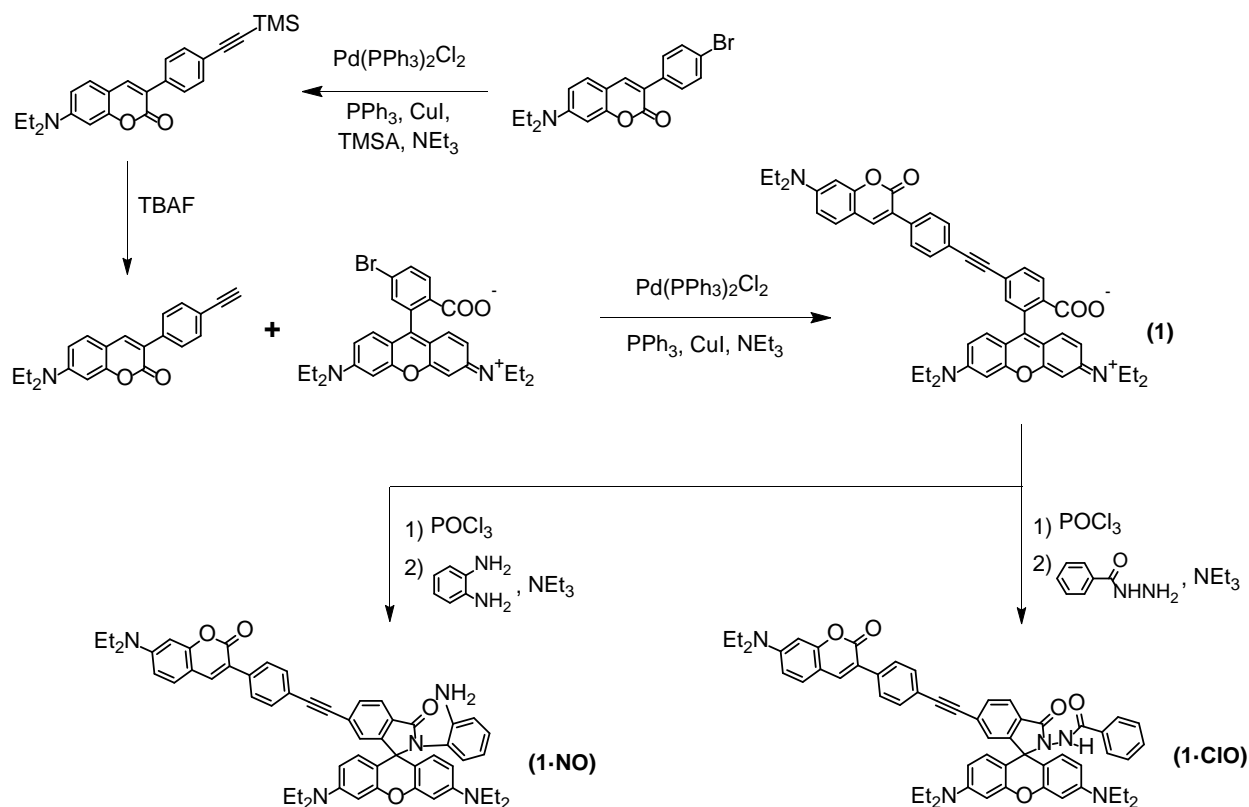
The authors declare no conflict of interest.

Keywords: Fluorescent Probes • Ratiometric • Through Bond Energy Transfer • Nitric Oxide • Hypochlorite

- [1] a) D. W. Domaille, E. L. Que and C. J. Chang, *Nat. Chem. Biol.* **2008**, *4*, 168-175; b) L. D. Lavis and R. T. Raines, *ACS Chem. Biol.* **2008**, *3*, 142-155; c) T. Ueno and T. Nagano, *Nat. Methods* **2011**, *8*, 642-645.
- [2] a) A. P. Demchenko, *J. Fluoresc.* **2010**, *20*, 1099-1128; b) J. Fan, M. Hu, P. Zhan and X. Peng, *Chem. Soc. Rev.* **2013**, *42*, 29-43; c) R. Zhang, F. Yan, Y. Huang, D. Kong, Q. Ye, J. Xu and L. Chen, *RSC Adv.* **2016**, *6*, 50732-50760.
- [3] a) J. S. Kim and D. T. Quang, *Chem. Rev.* **2007**, *107*, 3780-3799; b) L. Yuan, W. Lin, K. Zheng and S. Zhu, *Acc. Chem. Res.* **2013**, *46*, 1462-1473.
- [4] a) G.-S. Jiao, L. H. Thoresen and K. Burgess, *J. Am. Chem. Soc.* **2003**, *125*, 14668-14669; b) R. Bandichhor, A. D. Petrescu, A. Vespa, A. B. Kier, F. Schroeder and K. Burgess, *J. Am. Chem. Soc.* **2006**, *128*, 10688-10689; c) W. Lin, L. Yuan, Z. Cao, Y. Feng and J. Song, *Angew. Chem. Int. Ed.* **2010**, *49*, 375-379.
- [5] a) M. Kumar, N. Kumar, V. Bhalla, H. Singh, P. R. Sharma and T. Kaur, *Org. Lett.* **2011**, *13*, 1422-1425; b) V. Bhalla, Roopa, M. Kumar, P. R. Sharma and T. Kaur, *Inorg. Chem.* **2012**,

- 51, 2150-2156; c) Y. J. Gong, X. B. Zhang, C. C. Zhang, A. L. Luo, T. Fu, W. Tan, G. L. Shen and R. Q. Yu, *Anal. Chem.* **2012**, *84*, 10777-10784; d) B. Yang and W. Wu, *Anal. Methods* **2013**, *5*, 4716-4722; e) S. Goswami, S. Paul and A. Manna, *RSC Adv.* **2014**, *4*, 43778-43784; f) C. Wang, D. Zhang, X. Huang, P. Ding, Z. Wang, Y. Zhao and Y. Ye, *Talanta* **2014**, *128*, 69-74; g) Y. R. Zhang, N. Meng, J. Y. Miao and B. X. Zhao, *Chem. Eur. J.* **2015**, *21*, 19058-19063; h) N. R. Chereddy, M. V. N. Raju, B. M. Reddy, V. R. Krishnaswamy, P. S. Korrapati, B. J. M. Reddy and V. J. Rao, *Sensors Actuat. B-Chem.* **2016**, *237*, 605-612; i) X. Han, L. Zhao, D. E. Wang, J. Xu, L. Zhang, M. S. Yuan, Q. Tu and J. Wang, *Analyst* **2016**, *141*, 1098-1104; j) S. L. Shen, J. Y. Ning, X. F. Zhang, J. Y. Miao and B. X. Zhao, *Sensors Actuat. B-Chem.* **2017**, *244*, 907-913.
- [6] a) H. Yu, Y. Xiao, H. Guo and X. Qian, *Chem. Eur. J.* **2011**, *17*, 3179-3191; b) H. Yu, L. Jin, Y. Dai, H. Li and Y. Xiao, *New J. Chem.* **2013**, *37*, 1688-1691.
- [7] J. Fan, P. Zhan, M. Hu, W. Sun, J. Tang, J. Wang, S. Sun, F. Song and X. Peng, *Org. Lett.* **2013**, *15*, 492-495.
- [8] a) L. Zhou, X. Zhang, Q. Wang, Y. Lv, G. Mao, A. Luo, Y. Wu, Y. Wu, J. Zhang and W. Tan, *J. Am. Chem. Soc.* **2014**, *136*, 9838-9841; b) L. Zhou, Q. Wang, X. B. Zhang and W. Tan, *Anal. Chem.* **2015**, *87*, 4503-4507.
- [9] a) L. Yuan, W. Lin, Y. Xie, B. Chen and J. Song, *Chem. Commun.* **2011**, *47*, 9372-9374; b) L. Yuan, W. Lin, B. Chen and Y. Xie, *Org. Lett.* **2012**, *14*, 432-435; c) L. Yuan, W. Lin, Y. Xie, B. Chen and J. Song, *Chem. Eur. J.* **2012**, *18*, 2700-2706; d) X. Guan, W. Lin and W. Huang, *Org. Biomol. Chem.* **2014**, *12*, 3944-3949.
- [10] Y. W. Yap, M. Whiteman and N. S. Cheung, *Cell. Signal.* **2007**, *19*, 219-228.
- [11] Z. M. Prokopowicz, F. Arce, R. Biedron, C. L. L. Chiang, M. Ciszek, D. R. Katz, M. Nowakowska, S. Zapotoczny, J. Marcinkiewicz and B. M. Chain, *J. Immunol.* **2010**, *184*, 824-835.
- [12] a) S. Weitzman and L. Gordon, *Blood* **1990**, *76*, 655-663; b) C. C. Winterbourn and A. J. Kettle, *Free Radi. Biol. Med.* **2000**, *29*, 403-409; c) S. Sugiyama, Y. Okada, G. K. Sukhova, R. Virmani, J. W. Heinecke and P. Libby, *Am. J. Pathol.* **2001**, *158*, 879-891; d) D. I. Pattison and M. J. Davies, *Biochem.* **2006**, *45*, 8152-8162.

- [13] a) S. H. Snyder, *Science* **1992**, 257, 494-496; b) D. Fukumura, S. Kashiwagi and R. K. Jain, *Nat. Rev. Cancer* **2006**, 6, 521-534; c) M. J. Rose and P. K. Mascharak, *Curr. Opin. Chem. Biol.* **2008**, 12, 238-244.
- [14] L. J. Ignarro, G. M. Buga, K. S. Wood, R. E. Byrns and G. Chaudhuri, *Proc. Natl. Acad. Sci.* **1987**, 84, 9265-9269.
- [15] a) C. Napoli and L. J. Ignarro, *Nitric Oxide* **2001**, 5, 88-97; b) S. P. L. Cary, J. A. Winger, E. R. Derbyshire and M. A. Marletta, *Trends Biochem. Sci.* **2006**, 31, 231-239; c) S. Yuan, R. P. Patel and C. G. Kevil, *Am. J. Physiol. Lung Cell. Mol. Physiol.* **2015**, 308, 403-415.
- [16] B. Zhu, C. Gao, Y. Zhao, C. Liu, Y. Li, Q. Wei, Z. Ma, B. Du and X. Zhang, *Chem. Commun.* **2011**, 47, 8656-8658.
- [17] a) H. Zheng, G. Q. Shang, S. Y. Yang, X. Gao and J. G. Xu, *Org. Lett.* **2008**, 10, 2357-2360; b) E. Sasaki, H. Kojima, H. Nishimatsu, Y. Urano, K. Kikuchi, Y. Hirata and T. Nagano, *J. Am. Chem. Soc.* **2005**, 127, 3684-3685.
- [18] a) Y. K. Yang, H. J. Cho, J. Lee, I. Shin and J. Tae, *Org. Lett.* **2009**, 11, 859-861; b) Z. Zhang, C. Deng, L. Meng, Y. Zheng and X. Yan, *Anal. Methods* **2015**, 7, 107-114.
- [19] H. Yu, Y. Xiao and H. Guo, *Org. Lett.* **2012**, 14, 2014-2017.



Scheme 1. Synthetic route of coumarin-rhodamine ratiometric dyads (**1**) for the detection of nitric oxide and hypochlorite.

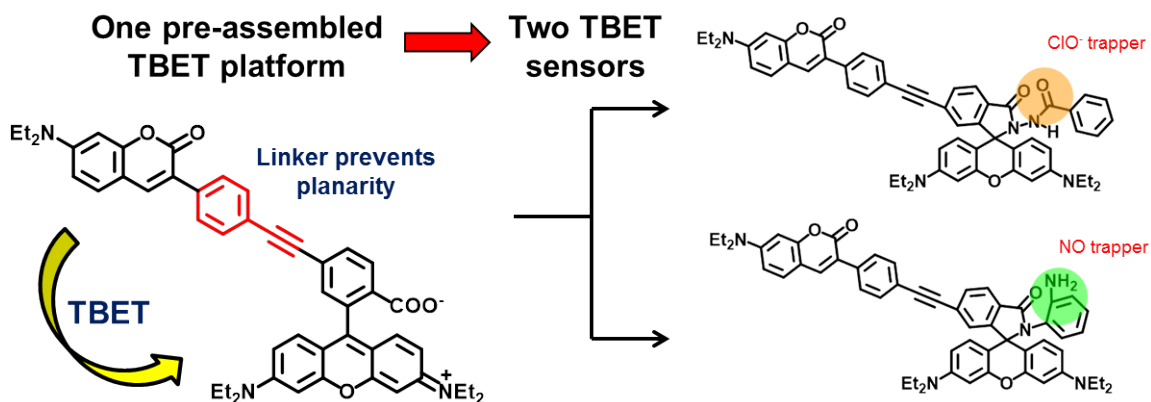


Figure 1. Design of a new coumarin-rhodamine TBET ratiometric platform and its applications for ratiometric sensing of nitric oxide and hypochlorite.

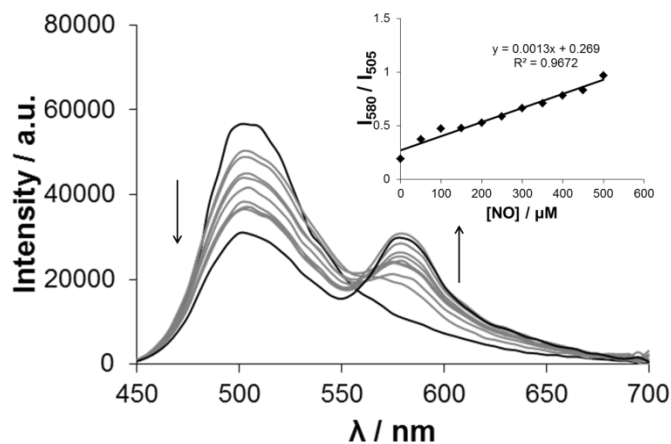


Figure 2. (a) Fluorescence spectra of **1•NO** (10 μM) in response to the presence of NO (DEA NONOate) (0–50 eq.) in $\text{CH}_3\text{CN}/\text{PBS}$ buffer ($v/v=4:6$, 2 mM, pH 7.4) ($\lambda_{\text{ex}}=420$ nm). Inset showing the linear plot of fluorescence intensity ratios (I_{580}/I_{505}) against NO concentrations.

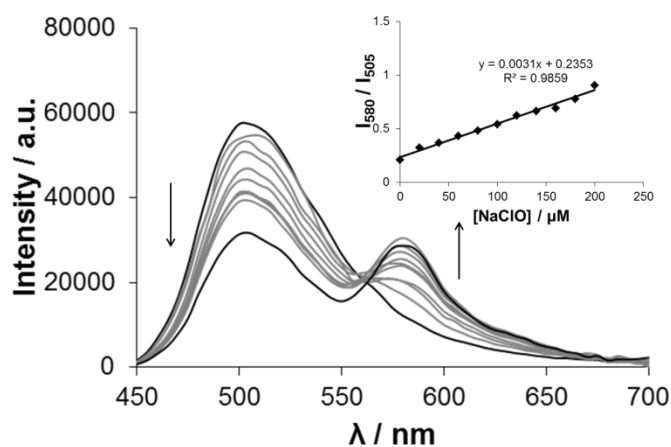


Figure 2. (b) Fluorescence spectra of **1•ClO** (20 μM) in response to the presence of NaClO (0–10 eq.) in $\text{CH}_3\text{CN}/\text{Tris-HCl}$ buffer ($v/v=6:4$, 2 mM, pH 7.4) ($\lambda_{\text{ex}}=420$ nm). Inset showing the linear plot of fluorescence intensity ratios (I_{580}/I_{505}) against NaClO concentrations.

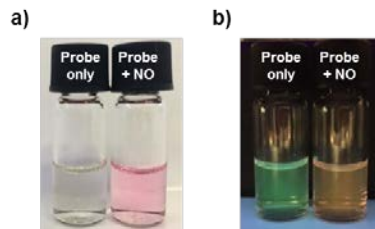


Figure 3. (a) Colour change before and after the addition of NO to $1\cdot\text{NO}$. (b) Fluorescence change before and after the addition of NO to $1\cdot\text{NO}$.

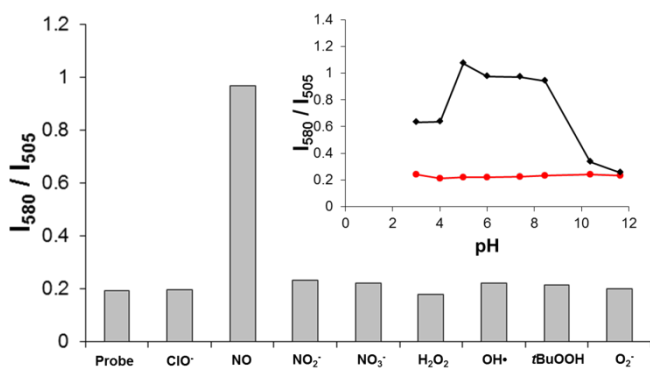


Figure 4. (a) Fluorescence responses (I_{580}/I_{505}) of $1\cdot\text{NO}$ (10 μM) upon addition of NO (DEA NONOate) and other ROS/RNS in $\text{CH}_3\text{CN}/\text{PBS}$ buffer ($v/v=4:6$, 2 mM, pH 7.4). Inset: Fluorescence responses (I_{580}/I_{505}) of $1\cdot\text{NO}$ (10 μM) against pH in the absence (\bullet) and presence (\blacklozenge) of NO (DEA NONOate).

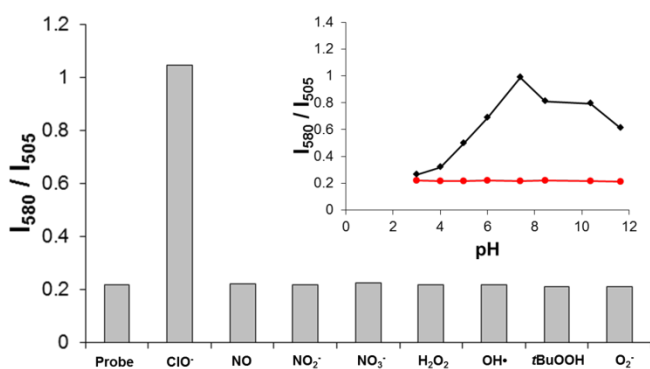


Figure 4. (b) Fluorescence responses (I_{580}/I_{505}) of $1\cdot\text{ClO}$ (20 μM) upon addition of NaClO and other ROS/RNS in $\text{CH}_3\text{CN}/\text{Tris-HCl}$ buffer ($v/v=6:4$, 2 mM, pH 7.4). Inset: Fluorescence responses (I_{580}/I_{505}) of $1\cdot\text{ClO}$ (20 μM) against pH in the absence (\bullet) and presence (\blacklozenge) of NaClO.

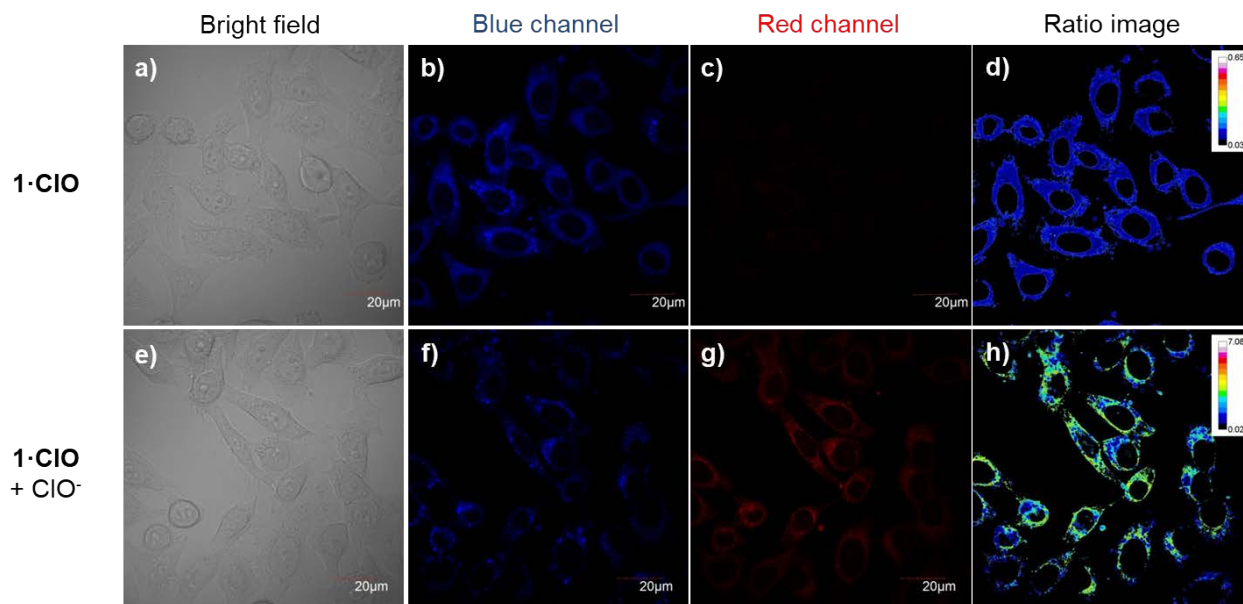


Figure 5. Confocal images of HeLa cells treated with **1•ClO** in the absence and presence of NaClO. (a) Bright field image of HeLa cells treated with **1•ClO** (20 μM) only; (b) Fluorescence image of (a) in the blue channel; (c) Fluorescence image of (a) in the red channel; (e) Bright field image of HeLa cells treated with **1•ClO** (20 μM) for 30 min and then further incubation with NaClO (100 μM) for 1 h at 37 °C; (f) Fluorescence image of (e) in the blue channel; (g) Fluorescence image of (e) in the red channel. (d) & (h) Ratio images of red and blue channels. $\lambda_{\text{ex}} = 405$ nm.

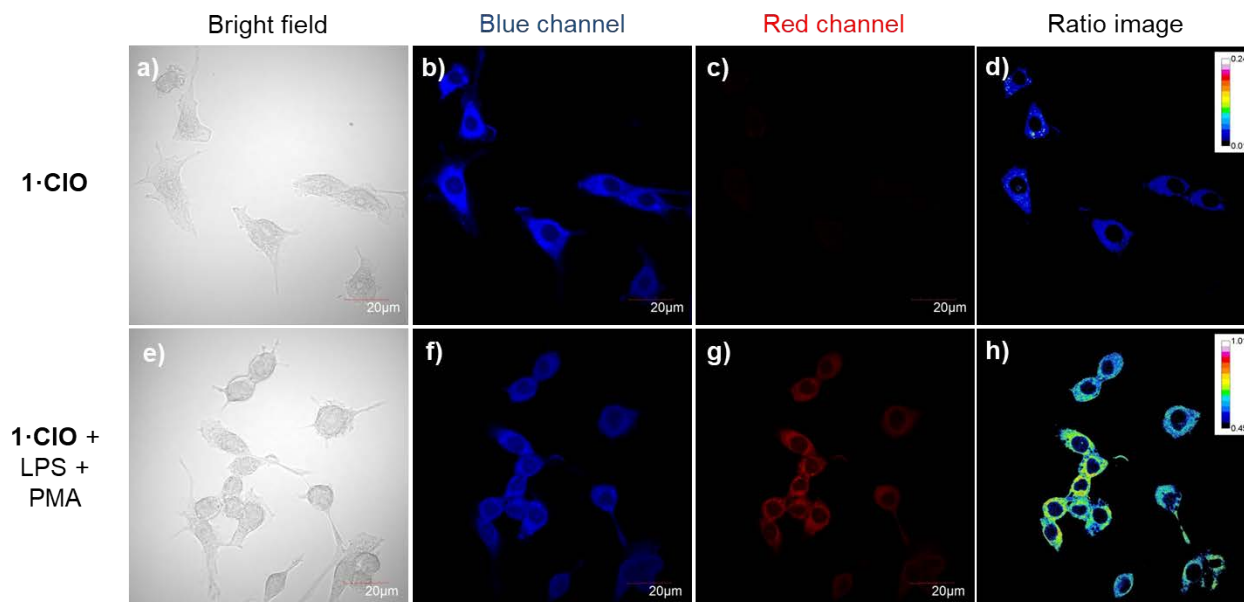
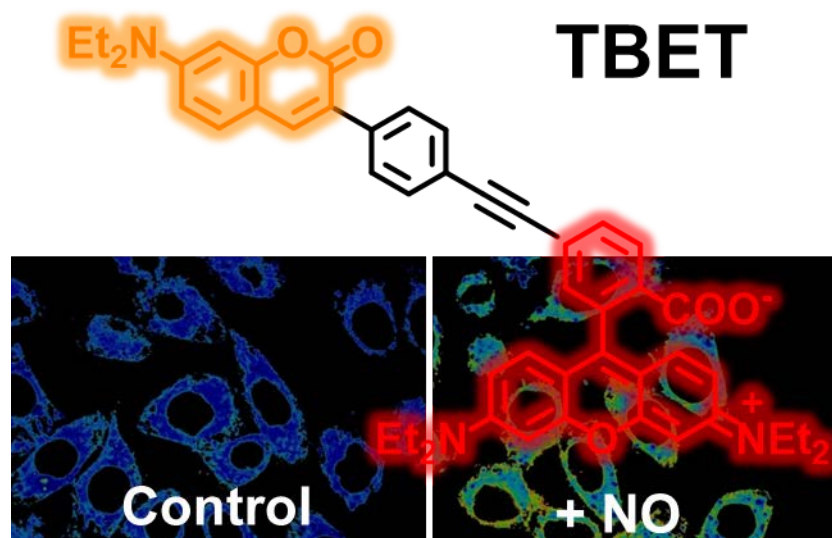


Figure 6. Confocal images of RAW 264.7 cells treated with **1•CIO** in the absence and presence of LPS and PMA. (a) Bright field image of RAW 264.7 cells treated with **1•CIO** (20 μM) only; (b) Fluorescence image of (a) in the blue channel; (c) Fluorescence image of (a) in the red channel; (e) Bright field image of RAW 264.7 cells treated with LPS (1 μg mL⁻¹) for 12 h and then further co-incubation with PMA (1 μg mL⁻¹) and **1•CIO** (20 μM) for 12 h at 37 °C; (f) Fluorescence image of (e) in the blue channel; (g) Fluorescence image of (e) in the red channel. (d) & (h) Ratio images of red and blue channels. $\lambda_{\text{ex}} = 405$ nm.

TOC graphic



Fluorescent ratiometric platform: A pre-assembled ratiometric scaffold based on TBET mechanism was developed to serve as a versatile chemosensor platform for the ready incorporation of various recognition motifs through facile amide coupling chemistry.